Application of EM Holographic Methods to Borehole Vertical Electric Source Data to Map a Fuel Oil Spill

L. C. Bartel, Sandia National Laboratories, Albuquerque, NM

SUMMARY

The multifrequency, multisource holographic method used in the analysis of seismic data is to extended electromagnetic (EM) data within the audio frequency range. The method is applied to the secondary magnetic fields produced by a borehole, vertical electric source (VES). The holographic method is a numerical reconstruction procedure based on the double focusing principle for both the source array and the receiver array. The approach used here is to Fourier transform the constructed image from frequency space to time space and set time equal to zero. The image is formed when the in-phase part (real part) is a maximum or the out-of-phase (imaginary part) is a minimum; *i.e.*, the EM wave is phase coherent at its origination. In the application here the secondary magnetic fields are treated as scattered fields. In the numerical reconstruction, the seismic analog of the wave vector is used; *i.e.*, the imaginary part of the actual wave vector is ignored. The multifrequency, multisource holographic method is applied to calculated model data and to actual field data acquired to map a diesel fuel oil spill.

INTRODUCTION

For the borehole-to-surface and cross-borehole electromagnetic (EM) method under consideration here, the primary EM field is produced by a grounded, borehole, vertical electric source (VES). The VES for cross-borehole magnetometric resistivity (MMR) measurements has been suggested and used by others (Edwards *et al.*, 1984; Nabighian *et al.*, 1984) where generally the VES is operated at a single frequency. In addition borehole-to-surface measurements (using the VES as a source of the primary EM field while measuring the horizontal magnetic fields at the surface) offers additional data that can be used to map the target of interest. The borehole-to-surface method was used by Bartel and Newman (1991) to map an injected salt water plume. The frequency in the MMR case is low enough such that the out-of-phase (imaginary) component is small. However as was shown by Bartel (1992) and as will be shown here, there is an advantage to operating over a range of frequencies such that the wave migration and extrapolation method (Bartel, 1992) and the holographic method, discussed below, can be applied to the analysis of data.

For a borehole VES in the earth operating in the audio frequency range (neglecting displacement currents) with an electrical structure which is axially symmetric about the VES, only a magnetic field (**H**) concentric with the VES is created and this field is completely confined to within the earth. In other words, there is no vertical H field created in the earth or in the air. Furthermore, since $\nabla\times\mathbf{H}=0$ (quasi-static limit) in air it can easily be shown that no horizontal **H** fields are created in the air. The presence of a geoelectric section which is not axially symmetric about the VES produces secondary **H** fields. The measured vertical **H** fields in a borehole or on the earth's surface and the measured horizontal **H** fields on the earth's surface are a result of the secondary **H** fields. The advantage of using the borehole VES is that the non-axially symmetric geoelectric section produces the desired response and the host response is minimized.

In this paper the EM holographic method, based on the work of Wu and Toksoz (1987) is successfully used to image a target using data from model calculations. With this success, the method is used to image a diesel fuel oil spill which occurred at a California site. The EM wave migration method (Bartel, 1992) and the EM holographic method discussed here are equivalent.

EM WAVES IN EARTH MATERIALS

The behavior of EM waves in earth materials was discussed briefly by Bartel (1992). From the solution to the Helmholtz equation in the frequency domain in the absence of sources, the complex wave vector in the quasi static limit is

$$k = [-i\omega\mu\sigma]^{1/2} \qquad (1)$$

where $\omega = 2\pi f$, f is the frequency, $\mu = \mu_r\mu_0$ (μ_r is the relative magnetic permeability and $\mu_0 = 4\pi\times10^{-7}$ H/m for the free space magnetic permeability), and σ is the electrical conductivity in S/m. The real part of k (k') gives rise to the propagation term and the imaginary part of k (k") gives rise to the damping term and are given by

$$|k'| = |k"| = [\omega\mu\sigma/2]^{1/2}. \qquad (2)$$

The phase velocity, v, defined from the dispersion relation $\omega = vk'$, and the wave length, λ, are given by

$$v = [2\omega/\mu\sigma]^{1/2}, \qquad \lambda = 2\pi v/\omega = 2\pi/k', \qquad (3)$$

respectively, which are both dependent upon $\sqrt{f}$ leading to dispersion.

HOLOGRAPHIC METHOD

Wu and Toksoz (1987) discussed both diffraction tomography and multisource holography applied to seismic imaging. Their approach has been adapted for EM waves in earth materials. Multisource holography is a generalization of the traditional single-source holography. It is a numerical reconstruction procedure based on the double focusing principle for both the source array and the receiver array. From Wu and Toksoz (1987) for any point (**x**) in the object space, the reconstructed image can be calculated using

$$I(\mathbf{x},\omega) = \sum_{m=1}^{M} B_s(r_s,r) \sum_{n=1}^{N} B_r(r,r_r)\, H_{mn} \quad (4)$$

where

$$B_r(r,r_r) = \exp[-ik'R_r(\mathbf{x})], \quad \text{and}$$
$$B_s(r_s,r) = \exp[-ik'R_s(\mathbf{x})]. \quad (5)$$

H_{mn} is a component of the scattered (secondary) magnetic field measured by the n-th receiver for the m-th source and is a function of frequency. B_r is the back propagator from the receiver point to the image point, B_s is the back propagator from the image point to the source point, R_r is the distance between the receiver and the image point, and R_s is distance between the source and the image point. Note, the back propagators are the same as the wave extrapolation operators used in wave migration. Here for the EM case, the magnitude of the wave vector, k', is given by equation (2) such that $k' = \omega/v$ which depends on the $\sqrt{f}$.

Equation (4) is an imaging process in that it focuses both the receiver array (inner summation) and the source array (outer summation) (Wu and Toksoz, 1987). To finalize the image condition: at time t=0 the **H** wave field is in phase with no (or very small) out-of-phase part; *i.e.*, at the origination of the wave field $\mathrm{Im}[I(\mathbf{x},t=0)] \approx 0$. To obtain $I(\mathbf{x},t=0)$, $I(\mathbf{x},\omega)$ is Fourier transformed from ω-space to t-space and time t is set to zero. For n discrete frequencies, $I(\mathbf{x},t=0)$ is given by

$$I(\mathbf{x},t=0) = (1/2\pi) \sum_{j=1}^{n} \Delta\omega_j\, I(\mathbf{x},\omega_j). \quad (6)$$

The image is formed when the magnetic field is in phase; *i.e.*, when $\mathrm{Re}[I(\mathbf{x},t=0)]$ is a maximum and/or when $\mathrm{Im}[I(\mathbf{x},t=0)] \approx 0$ or at least a minimum. The image $I(\mathbf{x},t=0)$ represents the field strength at the point of the scatterer and is a result of the secondary currents.

From Wu and Toksoz (1987), multifrequency, multisource holography is equivalent to prestack migration. Thus for the EM case, the multifrequency multisource holography is equivalent to the wave migration reported previously (Bartel, 1992).

MODEL CALCULATION

The multifrequency, multisource holography discussed above is applied to model calculations for the geoelectric model shown in Figure 1. This model was chosen so that a comparison to the wave migration method can be made (Bartel, 1992). The horizontal **H** fields were calculated using an integral equation method (Newman *et al.*, 1986) for the VES's shown in the figure. The fields were calculated over the frequency spectrum from 4 Hz to 4096 Hz in binary steps. The **H** fields provided the input for the field components $H(\mathbf{x},\omega)_{mn}$. For the model shown in Figure 1, the horizontal components of **H** were combined to give a magnitude and phase of the horizontal magnetic field. This was accomplished by determining the magnitude of the real and imaginary parts and then determining the phase from the real and imaginary parts. It is this horizontal field which was used an the input H_{mn} in equation (4).

The $|\mathrm{Re}[I(t=0)]|$ hologram is shown in Figure 2 where a resistivity of 10 Ω.m was used to calculate k' used in equation (5) giving a constant velocity at a given frequency. Shown is a cross-section at x = 0 along the y-axis (see Figure 1). For the hologram six frequencies were used, 128 Hz to 4096 Hz in binary steps. The imaged area was divided into 5 x 5 m grid from the surface to 50 m deep and from y = -20 to 20 m. The hologram was formed from data calculated at 25 surface data stations for the three transmitters (75 data points in all). The lighter shades of gray are areas where $|\mathrm{Re}[I(t=0)]|$ is larger, the darker shades is where $|\mathrm{Re}[I(t=0)]|$ is smaller. The area where $|\mathrm{Re}[I(t=0)]|$ is a maximum is the area of maximum phase coherency and is the source of the secondary magnetic fields. Shown in the figure is the location of the target used for the calculations. It is noted that the area with a maximum $|\mathrm{Re}[I(t=0)]|$, "white area", is offset to a slightly shallower depth and is centered at y = -2.5 m instead of y = 0 as in the model calculations. The area where $|\mathrm{Re}[I(t=0)]|$ is a maximum is centered at a depth of approximately 25 m to be compared to the actual depth of 30 m to the top of the target.

The agreement between the holographic reconstruction and the actual target is reasonable. Some error in the target depth may be a result of the long bipole electrical source (see Figure 1). The effects of the length of the VES on target definition is under investigation. In addition, target resolution is limited by the frequencies used for the reconstruction. For example, at 4096 Hz the wave length is 156 m for 10 Ω.m earth material which is approximately 13 times longer than the width of the target. For the frequencies used, the target is detected but the resolution of the target is limited; however, the resolution is better than one might think based on the wave lengths involved because of the focusing action of the holographic method. The phase shift difference between using a uniform 10 Ω.m rather than the actual layers (see Figure 1) is insignificant. It is noteworthy that the wave migration method (Bartel, 1992) produced an image of H_y at a depth of approximately 25 m using the same model calculations and only one transmitter.

VES EXPERIMENT

In the fall of 1992, a VES EM experiment was planned and executed at a fuel oil spill (FOS) site at the Sandia National Laboratories (SNLL) installation in Livermore, CA. In February 1975, a 225.2 m^3 (59,500 gal.) spill of No. 2 diesel fuel resulted from the accidental puncture of an underground transfer line buried about 1.2 m below the land surface. Some of the diesel fuel infiltrated the soil underlying the spill site; the remainder migrated laterally in a shallow trench adjacent to the spill where it is thought to have migrated vertically and laterally below the trench into the unconsolidated soil column. A small amount of fuel oil was recovered from the shallow trench near the puncture; however, an evaluation of the site indicated that 162 m^3 (43,000 gal.) of diesel oil remains in the unsaturated zone. For more information the reader is referred to DOE (1989).

Figure 3 shows the layout of surface data stations, the location of the four transmitter/receiver wells, and one of the monitor wells. The spill release point is also shown in the figure. The surface data stations are on a 10 x 10 m grid for a total of 49 surface data stations. For the four transmitter/receiver wells, four VES electrodes were installed on the outside of PVC casing at a spacing of 9.144 m with the bottom electrode at a depth of 31.85 m. Five of the six possible transmitter configurations in each well were used (the one not used was the one using the total length). Data were taken at the 49 surface data stations, along with six vertical magnetic field (H_z) measurements in each of the four boreholes for the 20 transmitters. In addition, the vertical electric field (E_z) was measured in the boreholes not being used for the transmitter. The frequency range used was 16 Hz to 4096 Hz in binary steps.

APPLICATION OF THE HOLOGRAPHIC METHOD

The |Re[I(t=0)]| hologram is shown in Figure 4 for a cross-section at x = 35 m along the y-axis (see Figure 3). A resistivity of 40 Ω.m was used to calculate k' in the back propagators. For the hologram three frequencies were used, 1024 Hz to 4096 Hz in binary steps. The imaged area was divided into 5 x 5 m grid from the surface to 50 m deep and from y = 0 to 60 m. The hologram was formed from data measured at 49 surface data stations for the 20 distinct transmitters (980 data points in all). The lighter shades of gray are areas where |Re[I(t=0)]| is larger, the darker shades is where |Re[I(t=0)]| is smaller. It is noted that the area with a maximum |Re[I(t=0)]|, "white area", is centered at a depth of 5 m and centered at a y distance of 40 m. This area with a maximum |Re[I(t=0)]| is the area of maximum phase coherency and is the source of the measured secondary magnetic fields.

Figure 5 shows the |Re[I(t=0)]| hologram for a plan view at a depth of 5 m. Again a 5 x 5 m grid was used for the imaged area. The same data stations, transmitters, and frequencies were used as were used to construct Figure 4. The area with a maximum |Re[I(t=0)]| is centered at x = 27.5 m and y = 40 m. The "X's" represent the locations of the transmitter wells and the "O" represents the location of the FTA well (see Figure 3). From an examination of Figure 3, the spill release point was at a location of approximately 2 m north of the FTA well (x = 33 m, y = 37 m). The end of the shallow trench was approximately 2 m west of the spill release point. The location of the maximum in |Re[I(t=0)]| agrees with the location of spill release point where the highest concentrations of the diesel fuel were measured (approximately 10,000 mg/kg). Areas of maximum |Re[I(t=0)]| are areas of the source of the secondary magnetic fields. The relationship between the image values and the conductivity is being investigated. The source of the secondary magnetic fields can be either a conducting anomaly or a resistive anomaly. In this case it is believed that the diesel fuel will produce a resistive anomaly.

For 40 Ω.m earth material, the wave length at 4096 Hz is 312 m. Here as for the model calculations, targets can be detected but the resolution is limited. Again the focusing action of the holographic improves the resolution somewhat. It is noteworthy that at a frequency of 4096 Hz in 40 Ω.m earth material, there is a 1.15 deg./m phase shift for an EM wave traveling through the earth.

The holograms from the cross-borehole data show similar results for the target location as do the borehole-to-surface results shown in Figures 4 and 5. For the sake of brevity, the discussion of the cross-borehole data will be deferred.

SUMMARY AND CONCLUSIONS

The multisource holographic method described by Wu and Toksoz (1987) for seismic imaging has been adapted for use on EM data. The holographic reconstruction of calculated model data are in good agreement with the actual model calculations. The EM holographic reconstruction was applied to VES EM data taken at a diesel fuel oil spill site. The reconstructed image agrees very well with the location of the spill release point where the majority of the fuel oil remains in the subsurface. For the frequencies used in the reconstructions the targets are detected; however, the resolution of the target is limited by the frequencies involved.

From the work done to date, areas of future research are apparent. The first is to relate the reconstructed image |Re[I(t=0)]| to the conductivity structure. The second is a methodology of combining borehole-to-surface and cross-borehole data to be able to utilize the total data set. On the experimental side, in order to gain resolution it will be necessary to operate at higher frequencies.

ACKNOWLEDGMENTS

The author wishes to thank P. M. Drozda, J. E. Uhl, and R. D. Jacobson (all with Sandia) for the expert technical assistance in the acquisition of the data. In addition, the author wishes to thank W. T. Hobson of SNLL for valuable assistance. The author also wishes to acknowledgments helpful discussions about the holographic method with M. W. Scott and S. A. Urquhart. This work performed at Sandia National Laboratories supported by the U.S. Department of Energy under contract DE-AC04-76DP00789.

REFERENCES

Bartel, L. C and Newman, G. A., 1991, Mapping a 3-D conductivity anomaly using a vertical electric source - field results: Expanded abstracts Society of Exploration Geophysicists annual meeting, Houston, TX, Nov. 10-14, 472-475.

Bartel, L. C., 1992, Application of wave migration to borehole vertical electric source EM data: Expanded abstracts Society of Exploration Geophysicists annual meeting, New Orleans, LA, Oct. 25-29, 506-510.

DOE, 1989, Sandia National Laboratories, Livermore, Fuel Oil Spill: U.S. Department of Energy, Albuquerque Operations Office, Environment and Health Division, ER Programs Project Group, April.

Edwards, R. N., Nobes, D. C, and Gomez-Trevino, E., 1984, Offshore electrical exploration of sedimentary basins - The effects of anisotropy in horizontally isotropic layered media: Geophysics, 49, 556-576.

Nabighian, M. N., Opplinger, G. L., Edwards, R. N., Lo, B. B., and Chessman, S. J., 1984, Cross-hole magnetometric resistivity (MMR): Geophysics, **49**, 1313-1326

Newman, G. A., Hohmann, G. W., and Anderson, W. L., 1986, Transient electromagnetic responses of a three dimensional body in a layered earth: Geophysics, **51**, 1608-1627.

Wu, R. S. and Toksoz, M. N., 1987, Diffraction tomography and multisource holograph applied to seismic imaging: Geophysics, **52**, 11-25.

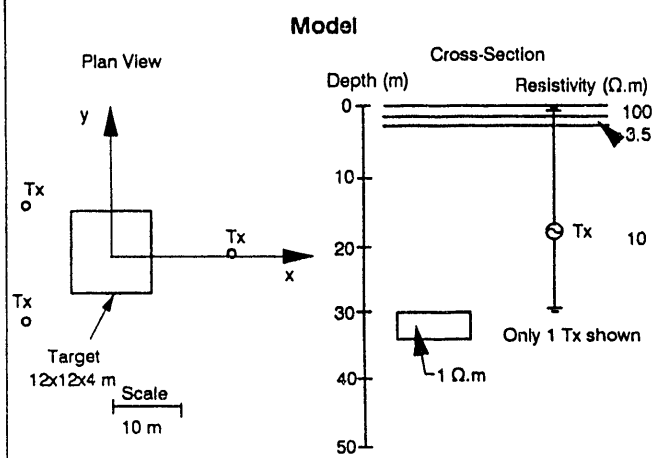

Fig. 1 Geoelectric model for model calculations.

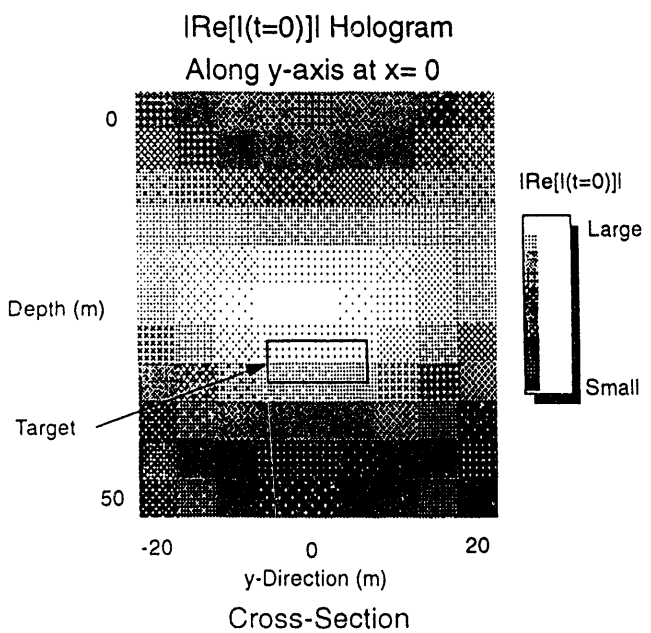

Fig. 2 Cross-section |Re[I(t=0)]| hologram from model calculations.

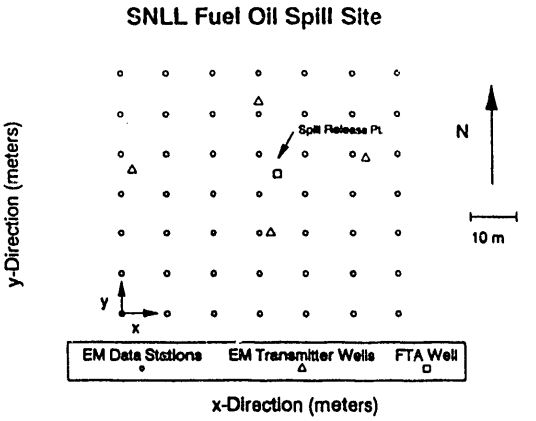

Fig. 3 Site map of the SNLL FOS site. The origin is in the lower left corner as indicated.

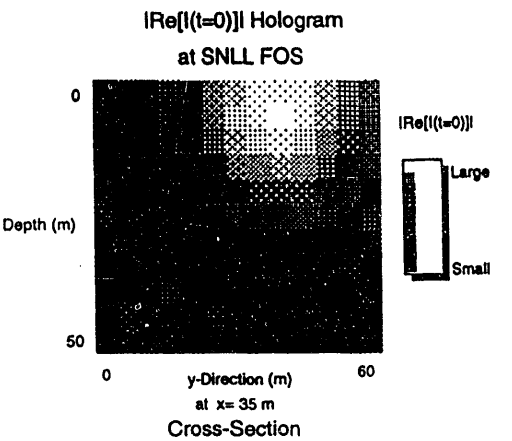

Fig. 4 Cross-section |Re[I(t=0)]| hologram for the SNLL FOS.

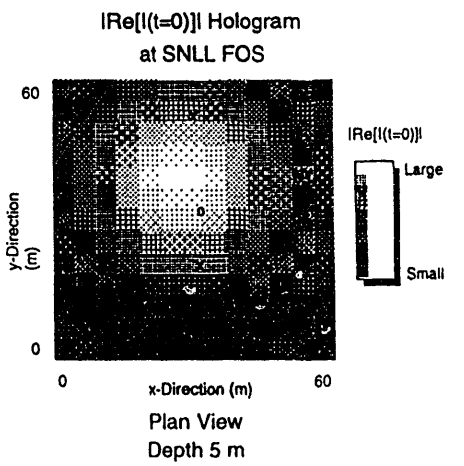

Fig. 5 Plan-view |Re[I(t=0)]| hologram for the SNLL FOS. The "X's" represent locations of the transmitting wells and the "O" represents the location of the FTA well.